Friction Stir Processing of Beta C and Ti-185: A Unique Pathway to Engineer Microstructures for Exceptional Properties in β Titanium Alloys

VEDAVYAS TUNGALA, ANIKET K. DUTT, DEEP CHOUDHURI, RAJIV S. MISHRA, SESH A. TAMIRISAKANDALA, KYU C. CHO, and RAYMOND E. BRENNAN

Metastable β titanium alloys offer a wide range of attractive property combinations. Conventional processing options have practical limitations in achieving maximum attainable properties and utilizing them to their fullest potential. In the current study, friction stir processing (FSP) of β alloys is explored as a unique path for microstructural engineering. Two metastable β titanium alloys, Ti-1Al-8V-5Fe (Ti-185) and Ti-3Al-8V-6Cr-4Mo-4Zr (Beta C), subjected to FSP with two different tool rotation rates at a constant traverse speed were analyzed in different microstructural conditions. Fully retained β grain structures with grain sizes in the range 4 to 7 μm in Ti-185 and 10 to 15 μm in Beta C were obtained in the as-FSP condition. Post-FSP duplex aging treatment of the low heat input condition resulted in better tensile properties compared to those of high heat input condition, attributable to high number density of nucleation sites generated during FSP. Transmission electron microscopy observations of high-strength Ti-185 sample revealed fine α platelets of length in the range 50 to 130 nm and an aspect ratio in the range 3 to 10, providing significant strengthening contribution. Approximate nose temperatures and nose time calculations of the continuous cooling transformation of β to α were made for various commercial Ti alloys to assess the potential of achieving ultra-high strength levels *via* FSP.

I. INTRODUCTION

SINCE the early 2000s, the use of titanium alloys in the aerospace, automotive, chemical, petrochemical, biomedical, and defense industries increased markedly due to their attractive properties such as lightweight (about 60 pct lighter than steels), excellent corrosion resistance, bio-compatibility, and good ballistic resistance.[1,2] In recent times, β titanium alloys have become widely explored candidates of choice because of their wide range of property combinations. Figure 1 illustrates the uses of β Ti alloys in various industries. Applications of β alloys are driven by significant weight savings due to superior specific strength (strength-to-weight ratio) leading to significant life-cycle cost savings. The primary challenge in the research and development of β alloys is to enhance strength while retaining acceptable fracture properties. Rapid grain growth in β alloys during conventional thermo-mechanical processing (TMP) due to high diffusion rates in the β phase and associated anisotropy constrains the maximum achievable mechanical properties and applications of β alloys. The current study explores the application of a novel deformation technique, friction stir processing (FSP), to β Ti alloys to overcome these issues.

FSP is currently used for many Al,[3–8] Mg,[9,10] and Cu[11] alloys. Progress in the application of FSP to Ti alloys has been slow due to limited availability of tool materials that can withstand high temperatures and loads generated during the process. Numerous authors have investigated the FSP of the workhorse $\alpha + \beta$ titanium alloy, Ti-6Al-4V (Ti-64), using tools such as W,[12,13] W-Re,[14–20] Mo-based,[21] polycrystalline boron nitride,[22] WC-Co,[23] and lanthanated W.[24] Recent works on FSP of titanium alloys show the enhanced mechanical properties due to microstructural evolution.[25–29] Studies on the FSP of β titanium alloys are scanty. Leinart *et al.*[30] studied the effect of FSP on the

VEDAVYAS TUNGALA, ANIKET K. DUTT, DEEP CHOUDHURI, and RAJIV S. MISHRA are with the Center for Friction Stir Processing, Department of Materials Science and Engineering, University of North Texas, Denton, TX 76207. Contact e-mail: Rajiv.Mishra@unt.edu SESH A. TAMIRISAKANDALA is with Arconic Titanium & Engineered Products, 1000 Warren Avenue, Niles, OH 44446. KYU C. CHO and RAYMOND E. BRENNAN are with the Weapons and Materials Research Directorate, U.S. Army Research Laboratory, Aberdeen Proving Grounds, MD 21005.
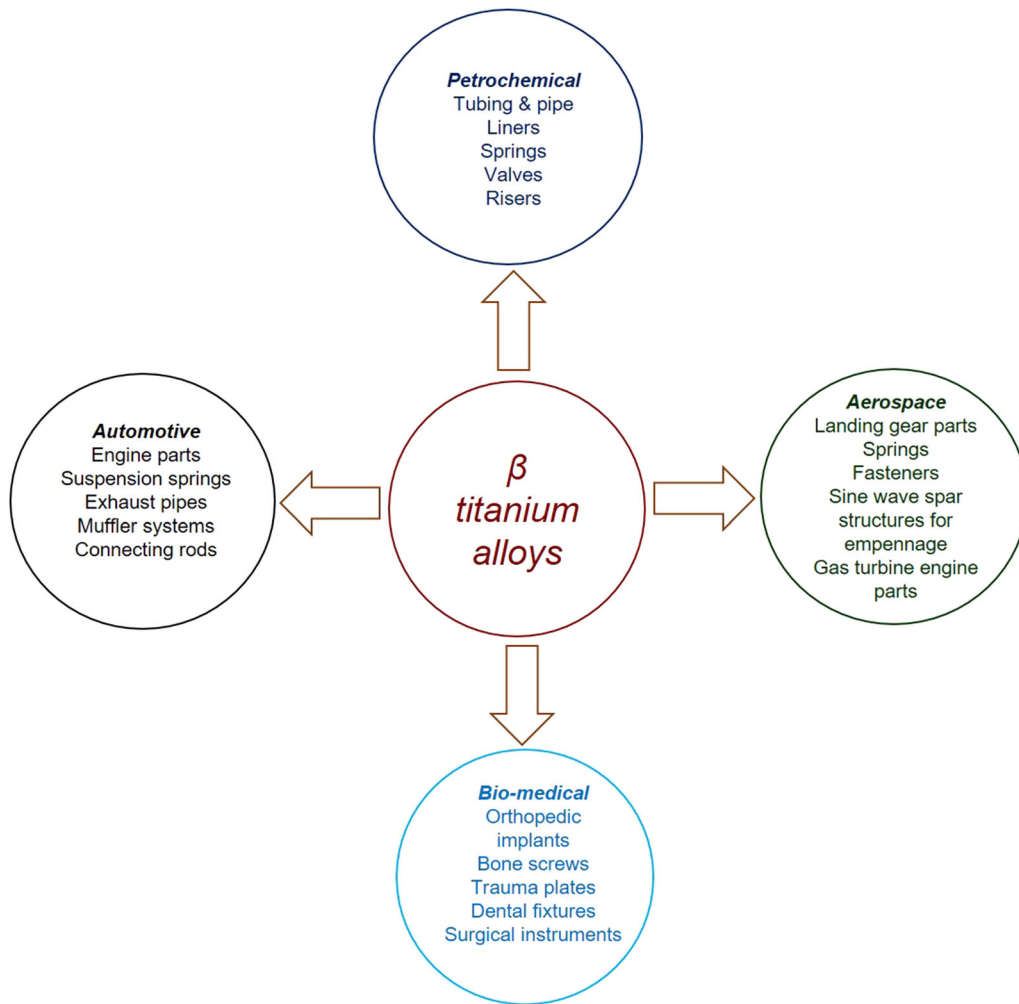
Fig. 1—Overview of the usage of β titanium alloys in various industries.

microstructure and mechanical properties of Ti-15V-3-Cr-3Al-3Sn (Ti-15-3), a metastable β alloy used in environmental control systems (*e.g.*, ducting on Boeing 777 and Airbus A380). A fully recrystallized β grain microstructure was obtained after FSP, with a grain size in the range 10 to 20 μm, developed as a result of dynamic recovery followed by meta-dynamic recrystallization.[30] Another study on Ti-15-3 reported the grain structure evolved through discontinuous recrystallization; the deduction was that the textural pattern in the stir zone was the superposition of (111) and (110) partial fiber textures.[31] Reynolds *et al.*[14] studied the texture in friction stir welds of Ti-15Mo-2.6Nb-3Al-0.2Si (Beta 21S). Fairly uniform texture through the thickness of the weld was reported. All the textures obtained could be rotated to obtain a BCC torsion texture published earlier. Increase in texture intensity with the decrease in tool traverse speed was observed.[14]

Current study focuses on developing a comprehensive processing–structure–property relationship in β Ti alloys using data generated on two commercial alloys, Ti-1Al-8V-5Fe (Ti-185) and Ti-3Al-8V-6Cr-4Mo-4Zr (Beta C), subjected to FSP. Ti-185 is a low-cost alternative to Ti-10V-2Fe-3Al (Ti-10-2-3), for potential aerospace fastener and structural applications.[32] Recent work on Ti-185 processed *via* powder metallurgy route demonstrated the feasibility of achieving exceptional strength levels, potential for many lightweighting applications, and improving fuel efficiency.[33] Beta C is a highly alloyed metastable β alloy primarily used for aerospace springs and fasteners, and tubulars in oil and gas industries.[32] The mechanical properties reported for these alloys are obtained *via* complex and expensive TMP sequences. The current study investigates FSP as a unique processing pathway with a goal of achieving tensile strength of 1500 MPa while maintaining minimum tensile elongation of 5 pct. Application of FSP to many other metastable β Ti alloys to achieve high strength–high ductility combinations is also investigated using continuous cooling transformation diagram calculations.

II. MATERIALS AND METHODS

Two commercial β Ti alloys, Ti-185 in the as-cast condition and Beta C in the as-forged condition, were used in this study. Alloy compositions (nominal and

program materials) are given in Table I. FSP was performed on both alloys using W-La$_2$O$_3$ tool with two varying heat input (Q) conditions given in Table II. The tool had a cylindrical pin with shoulder diameter of 10.1 mm, pin diameter of 6.3 mm, and pin length of 1.7 mm. FSP was performed with the tool at a tilt angle of 2.5 deg opposite to the processing direction. Argon gas shielding was used during FSP to prevent oxidation. The 600 rpm/2 ipm combination is hereafter referred to as low Q FSP and 800 rpm/2 ipm combination is referred to as high Q FSP.[34] Molybdenum equivalent [Mo]$_{eq}$ calculated using Eq. [1] (all elements in wt pct) and β transus temperature measured using differential thermal analysis with an accuracy of ± 5 °C are also given in Table II.

$$[Mo]_{eq} = [Mo] + \frac{2[V]}{3} + \frac{[Nb]}{3} + 3([Fe] + [Cr]) \quad [1]$$

Post-FSP heat treatment on processed regions of both alloys included two-step aging, with the pre-age cycle of 350 °C for 2 hours plus the final aging cycle of 540 °C for 8 hours followed by air cool to room temperature.

Macro- and microstructural characterization on the transverse cross sections of the processed regions was performed using optical microscopy and scanning electron microscopy (SEM). Metallographic specimens were prepared by grinding through 1200-grit SiC papers and final polishing using 0.05 μm colloidal silica. Specimens were etched with Kroll's reagent for optical and secondary electron SEM observations. Backscattered electron imaging was performed on as-polished specimens. Transmission electron microscopy (TEM) on selected samples was performed using a FEI Tecnai F20-FEG™ microscope operating at 200 kV.

Mini-tensile specimens of 3 mm gage length, 1 mm width, and 0.45 mm thickness were machined from the center of the stir zone along the FSP direction. All tensile tests were carried out at room temperature using a computer-controlled, custom-built mini-tensile testing machine at an initial strain rate of 1×10^{-3} s^{-1}.

III. RESULTS AND DISCUSSION

Macrographs of starting condition and nugget cross-section of Ti-185 and Beta C are shown in Figure 2. The starting structure in both alloys comprised of very large grains (of the order of several millimeters). FSP resulted in a refined structure in both alloys. Micrographs obtained in the stir zone (SZ) at a depth of 0.5 mm (top), 1 mm (middle), and 1.5 mm (bottom) from the FSP surface are presented in the following subsection.

A. Microstructure Evolution in the Stir Zone

A fully recrystallized β grain structure in the SZ after FSP for both conditions of Ti-185 as seen in Figure 3 indicates that the SZ experienced a peak temperature above the β transus during processing and the cooling rate after FSP is sufficient to quench in the β grain structure. Average β grain sizes measured through the thickness using linear intercept method for low Q condition of Ti-185 are 4 ± 0.4, 10 ± 1, and 7 ± 0.8 μm (Figure 3) at the top, middle, and bottom regions. Similarly, for high Q condition, they are 11 ± 1.3, 15 ± 1.4, and 10 ± 1.6 μm, respectively. Variation in the β grain sizes through the thickness is expected due to local variations in strain and temperatures caused by the tool shoulder during FSP.[35] The increase in recrystallized β grain size in high Q compared to the low Q is due to higher processing temperature and grain growth due to longer dwell time above the β transus temperature.[36]

Microstructural observations on Beta C are presented in Figure 4. Average β grain sizes measured for low Q FSP in this alloy are 3 ± 0.9, 5 ± 0.8, and 4 ± 0.7 μm at the top, middle, and bottom locations, respectively. For high Q FSP, they are 7 ± 0.9, 10 ± 1, and 11 ± 1.2 μm, respectively. Finer β grain sizes in Beta C compared to those of Ti-185 in both FSP conditions are expected from rich solute contents which decrease grain boundary mobility (solute drag effect).[37]

Table I. Chemical Compositions in Weight Percent of Materials Used for this Study

Alloy	Material	V	Al	Fe	O	N	C	Cr	Mo	Ti
Ti-185	nominal	7.5 to 8.5	0.8 to 1.5	4 to 6	0.25 to 0.5	0.07	0.05	—	—	bal.
	actual	7.9	1.5	5.02	0.343	0.004	0.008			bal.
Beta C	nominal	7.5 to 8.5	3 to 4	0.3	0.14	0.03	0.05	5.5 to 6.5	3.5 to 4.5	bal.
	actual	7.96	3.43	0.1	0.1	0.007	0.012	6.02	4.06	bal.

Nominal chemistries of both alloys are also included for reference.

Table II. FSP Parameters, β Transus Temperature, and [Mo]$_{eq}$ of Program Materials

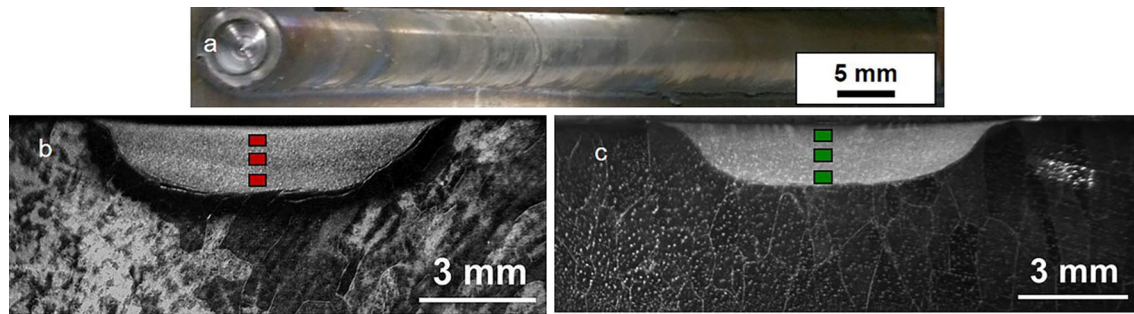| Alloy	Tool Rotation Speed (rpm)	Tool Traverse Speed (in./min)	FSP Condition	β Transus (°C)	[Mo]$_{eq}$
Ti-185	600	2	low Q	825	20.33
	800	2	high Q		
Beta C	600	2	low Q	795	27.33
	800	2	high Q		

Fig. 2—(a) Typical photograph of FSP region along the length and cross-sectional macrographs of (b) Ti-185 (left) and (c) Beta C (right). Microstructure samples were excised from the red and green box locations and are referred to as top, middle, and bottom regions of the stir zone (Color figure online).
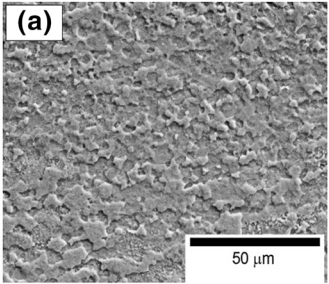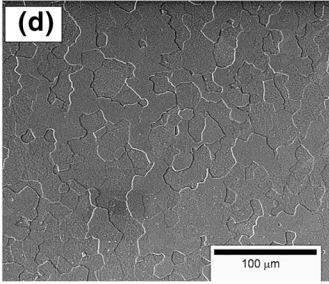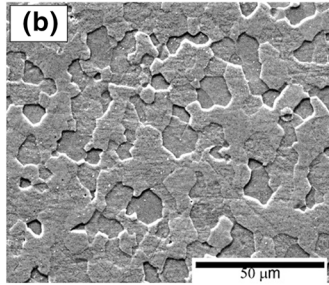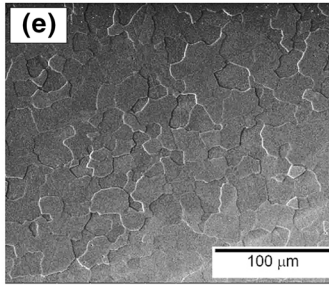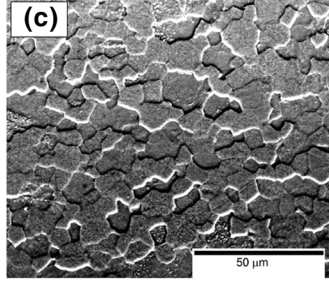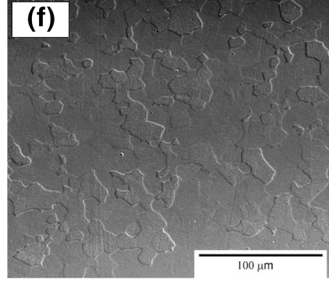

Fig. 3—Secondary electron images of Ti-185 samples in the as-FSP condition: (a through c) low Q and (d through f) high Q condition.

B. Tensile Properties in the As-FSP Condition

Table III presents a summary of room-temperature tensile properties of both Ti-185 and Beta C in the as-FSP conditions along with those of as-received (base metal) conditions. Significant increase in strength was obtained after FSP, which is attributable to the refined microstructure. In Ti-185, as heat input increases, the concomitant decrease in strength and ductility correlates with grain size. However, such a trend was not observed in Beta C.

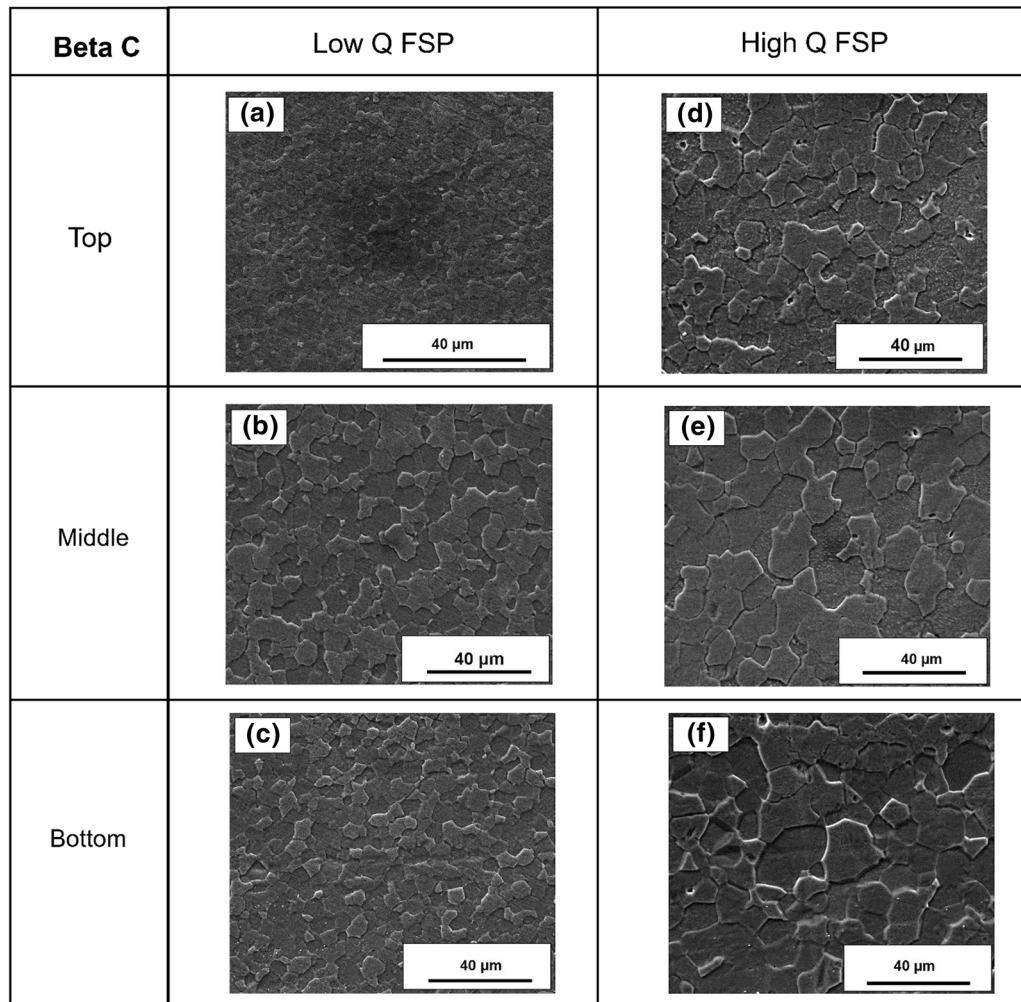| Beta C	Low Q FSP	High Q FSP
Top	(a)	(d)
Middle	(b)	(e)
Bottom	(c)	(f)

Fig. 4—Secondary electron images of Beta C samples in the as-FSP condition: (*a* through *c*) low *Q* and (*d* through *f*) high *Q* condition.

Table III. Room-Temperature Tensile Properties of Ti-185 and Beta C in Various Microstructure Conditions

Alloy	Condition	TYS (MPa)	UTS (MPa)	*e* (pct)
Ti-185	as received	993	999	11
	low Q FSP	1107	1125	19
	high Q FSP	1070	1088	14
	low *Q* FSP + age	1460	1523	5.7
	high *Q* FSP + age	1352	1450	6.7
Beta C	as received	812	816	15
	low Q FSP	900	925	19
	high Q FSP	1002	1043	19
	low *Q* FSP + age	1277	1315	9
	High *Q* FSP + age	1172	1200	9.5

TYS: 0.2 pct tensile yield strength, UTS: ultimate tensile strength, *e*: total tensile elongation.

C. *Effect of Aging on Microstructures*

To establish the influence of aging, a commonly used two-step aging cycle was applied on samples excised from FSP regions of both alloys. At first stage of aging, sample is aged at a low temperature to form the Omega phase, which acts as the nucleation site of alpha phase during the second stage of aging. Micrographs of Ti-185 and Beta C in both FSP conditions subjected to aging are presented in Figures 5 and 6. Homogeneous precipitation of α is evidenced in the low *Q* FSP condition of both alloys. For high *Q* FSP condition, coarse *β* grains, non-uniform precipitation, and precipitate-free zones are evident. The decrease in α volume fraction with an increase in *Q* can be explained as an effect of strain rate and temperature on the nucleation and growth kinetics.

The homogeneous precipitation of α leads to a reasonable inference that number density of nuclei at low *Q* FSP is comparatively higher than those of high *Q* condition in both alloys. This can be comprehended as follows. The deformation mechanisms in *β* titanium alloys have been reported to be dynamic recovery and/ or dynamic recrystallization.[38] Due to extremely high strain rates and temperatures during FSP, some regions of the microstructure are recrystallized; and the rest are still in dynamic recovery. This partially recovered microstructure is believed to be more in the low *Q* FSP compared to that of the high *Q* FSP sample consequently resulting in a more homogeneous microstructure for this heat input condition.
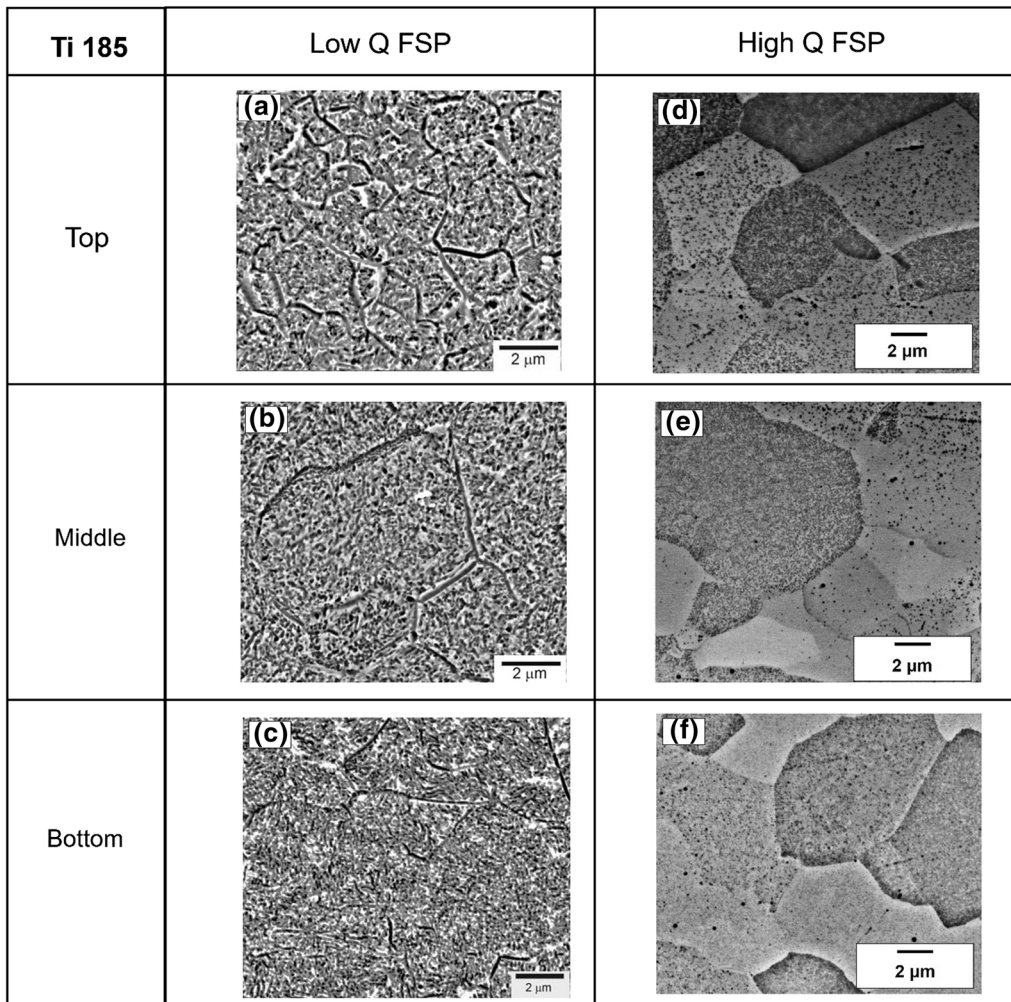
Ti 185	Low Q FSP	High Q FSP
Top	(a)	(d)
Middle	(b)	(e)
Bottom	(c)	(f)

Fig. 5—Backscattered electron images of Ti-185 samples in the FSP + age condition: (*a* through *c*) low *Q* FSP + age and (*d* through *f*) high *Q* FSP + age.

To further investigate the nature of precipitates responsible for high strength, TEM was conducted on the high-strength sample of Ti-185. A reasonable inference from HAADF-STEM image of Figure 7(a) is that several nanometer-sized platelets (appearing in darker contrast) in the range of 50 to 120 nm were uniformly distributed inside the β matrix. These precipitates were confirmed as hcp-α phase using [111] β selected area diffraction pattern (inset of Figure 7(b)) and exhibited the characteristic Burgers orientation relationship between α and β phases (shown with [11$\bar{2}$0] α and [111] β motifs in the SADP).[39] Figure 7 (b) shows size scale and morphology (viewed along [111] β) *via* dark-field TEM image, which was recorded with an α reflection. Our TEM examination did not reveal the presence of ω precipitates in this condition. Therefore, the precursory ω phases, which we anticipated would be formed in the pre-aging and would act as nucleating agents, were almost completely replaced by very fine alpha platelets in the final aging step. Hence the deduction that aging time and temperature were appropriate for Ti-185 to obtain a strength > 1500 MPa after

FSP, and these nano-scales α platelets were responsible for such a high strength in this alloy.

D. Characteristics of Stress–Strain Curves

Tensile properties of Ti-185 and Beta C after aging are compared with other conditions in Table III. Engineering stress–strain curves for the two alloys are shown in Figure 8. The peak stresses attained initially are higher for Beta C as compared to Ti-185. Stress–strain graphs further provide information about the non-uniform linear region, which is essentially termed as a strain-softened region, and is believed to occur in β titanium alloys in which rate of hardening by the generation of dislocations is balanced by the rate of softening due to dislocation annihilation.[30]

E. Strength Modeling

Strengthening mechanisms that contribute to the increase in tensile yield strength of metallic materials can be categorized as: solid solution strengthening (σ_{ss}),
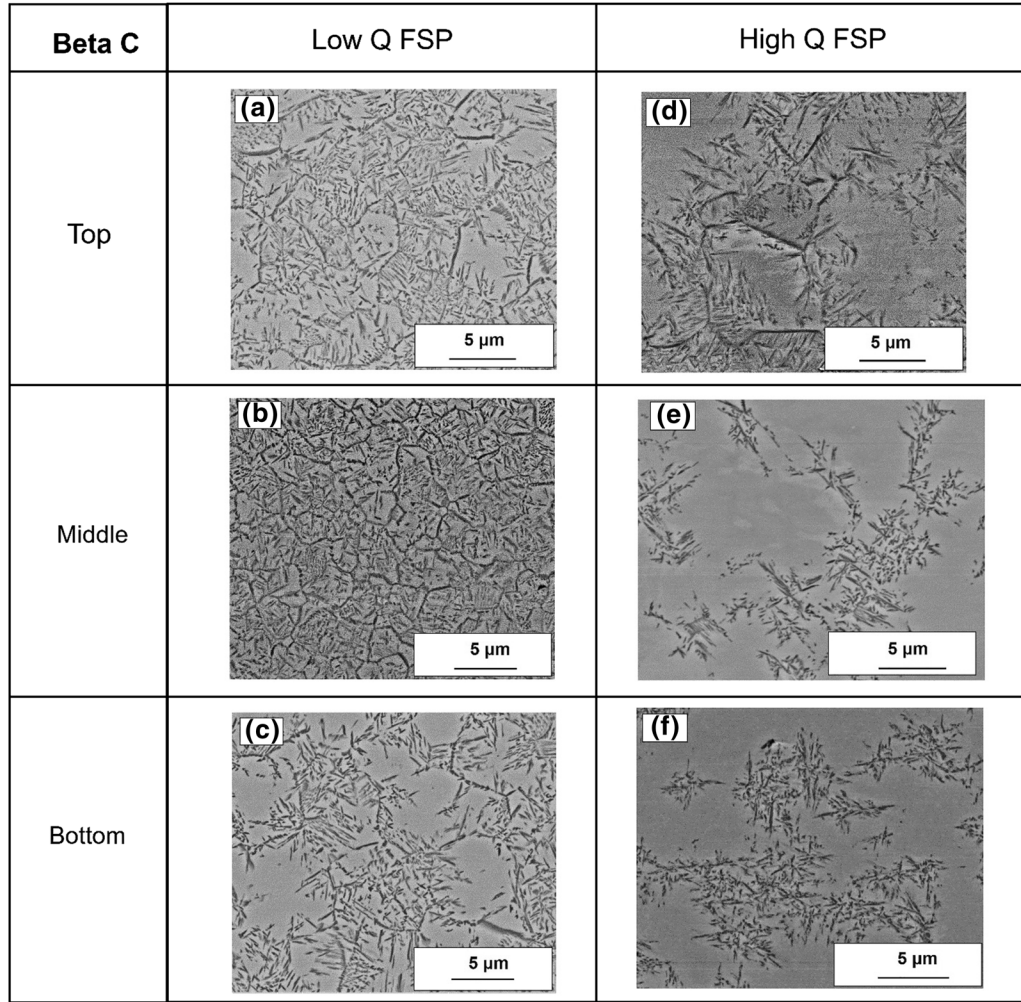
Beta C	Low Q FSP	High Q FSP
Top	(a)	(d)
Middle	(b)	(e)
Bottom	(c)	(f)

Fig. 6—Backscattered electron images of Beta C samples in the FSP + age condition: (a through c) low Q FSP + age and (d through f) high Q FSP + age.

grain size strengthening (σ_{gs}), precipitation strengthening (σ_{ps}), and dislocation strengthening (σ_{ds}). Assuming linear summation of these four mechanisms, total strengthening can be written as

$$\Delta\sigma_T = \sigma_{ss} + \sigma_{gs} + \sigma_{ps} + \sigma_{ds}. \qquad [2]$$

Equations for the above contributions can be written as follows.

Hall–Petch relationship grain size strengthening is given by[40,41]

$$\sigma_{gs} = kd^{-1/2}, \qquad [3]$$

where k is a constant taken as 0.41 from the reported result for Hall–Petch plot for β titanium alloys and d is the average grain size.

The dislocation strengthening contribution is expressed as[42]

$$\sigma_{ds} = M\tau_0 + M\alpha Gb\sqrt{\rho}, \qquad [4]$$

where M is the Taylor factor (= 3), α is a constant (0.5 to 0.58) determined from the plot σ vs $\rho^{1/2}$ for a β titanium

alloy,[42] ρ is dislocation density approximated as 10^{13} m^{-2} for the low Q condition and 10^{12} m^{-2} for the high Q condition.

The Peierls stress τ_0 can be calculated as follows:

$$\tau_0 = \frac{2G}{1 - v}\exp\left[\frac{-2\pi d}{(1 - v)b}\right], \qquad [5]$$

where G and b are considered for a β titanium alloy as 3.1×10^{10} Pa and 5.61×10^{10} m,[43] respectively, and d is the interplanar distance.

The solid solution strengthening contribution for each alloy was calculated based on the classic solid solution strengthening Eq. [6].[44] The solid solution strengthening contributions from each individual alloying element as per the alloy's nominal compositions were summed up to obtain the overall solid solution strength for each alloy.[45–47]

$$\sigma_{ss} = Gb\varepsilon^{\frac{3}{2}}c^n, \qquad [6]$$

where G is the shear modulus, c is the concentration of the solute atoms in wt pct, b is the Burger's vector, ε is the atomic misfit strain and n is considered as 0.5 for
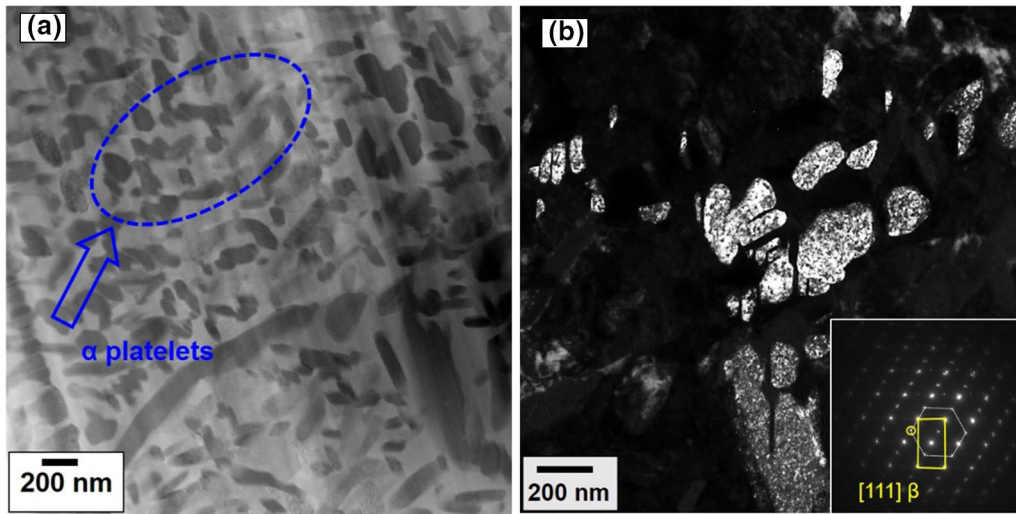
Fig. 7—(a) HAADF-STEM image of Ti-185 low Q FSP+age sample shows nano-scale α plates, and (b) dark-field image from [111] zone axis taken from SADP of the inset confirms the presence of alpha platelets of very fine size.
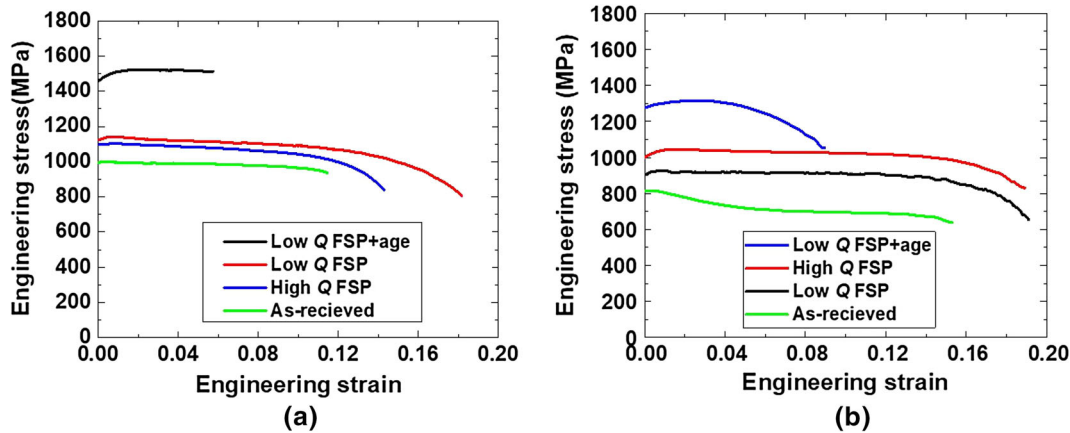

Fig. 8—Engineering stress–strain curves of (a) Ti185 and (b) Beta C relative to indicated processing conditions.

Table IV. Model and Experimental Tensile Yield Strengths for Beta C and Ti-185 in as-FSP Condition

Alloy	FSP Parameters	Avg. Grain Size, d (μm)	σ_{gs} (MPa)	σ_{ss} (MPa)	σ_{ds} (MPa)	σ_{YS} Model (MPa)	σ_{YS} Expt (MPa)	$\Delta\sigma_{YS}$ Expt-Model (MPa)
Ti185	low Q	7	155	453	204	812	1107	295
	high Q	12	119	453	184	756	1070	314
Beta C	low Q	4	205	518	184	907	927	20
	high Q	9.33	134	518	178	927	1002	172

interstitial solute atom and 1 for substitutional solute atom.[45,47]

Table IV summarizes the model strength predictions compared with experimental observations in as-FSP conditions. From this table, it can be inferred that for Beta C, the experimental and model strength difference is more in high Q condition as compared to that in the low Q condition. It has been reported that for Beta C, metastable phases such as β' and ω are expected to form

during cooling from above β transus temperature due to its complex alloying chemistry.[48,49] However, no signature of such phases is evident in SEM microstructures (if present they are too fine for SEM). A reasonable assumption is that these phases might have formed from auto aging that occurs during cooling after FSP. Also, highly probable is that because of its higher processing temperature, the high Q condition could retain more heat for longer time, compared to low Q, thus providing
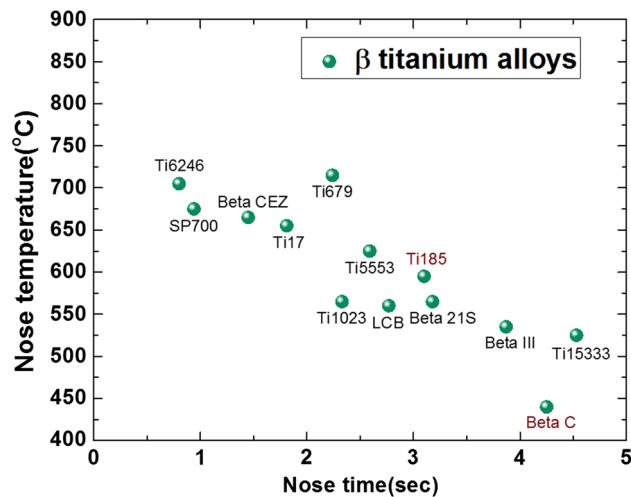
Fig. 9—Nose time *vs* nose temperature for all commercially available β-titanium alloys.

higher driving force for metastable phase formation leading to an increased strength with slightly reduced ductility.[50] In other words, the increase in strength in Beta C in the higher heat input condition is due to major contribution from the precipitation strengthening component of the metastable phases. In the case of Ti-185, although the precipitation strengthening contribution is more pronounced than Beta C (Table IV), there is no significant difference in these values between the two heat input conditions.

F. Nose time and nose temperature characteristics of β titanium alloys after FSP

The mechanical properties after FSP are better understood by studying continuous cooling transformation (CCT) diagrams. Empirical correlation from Yolton *et al.*,[51] shows nose temperature *vs* nose time plot of alpha precipitation for all commercially available β titanium alloys (Figure 9). This diagram gives the feasibility to quench in the β phase microstructure for all the β titanium alloys, which upon subsequent two-step aging gives rise to very high strength. The current alloys from this study are labeled in red. Nose time and nose temperature for Ti-185 are 3.1 seconds and 595 °C, respectively. Assuming the peak temperature in the friction stirred regions reached 1200 K (927 °C) and 1400 K (1127 °C), based on the assumption from Pilchak *et al.*,[52] the approximate cooling rate that is required to miss the nose temperature for the lower heat input condition should be > 107 °C s^{-1}; whereas for the higher heat input condition, it should be > 172 °C s^{-1}. Similarly, for Beta C, nose time and nose temperature are 4.25 seconds and 440 °C, respectively. Cooling rate calculations confirm that the approximate value should be > 114 °C s^{-1} for the higher heat input condition and that it should be > 162 °C s^{-1} for the lower heat input condition. The cooling rate involved for water quenching of Ti64 alloy is reported as 133 °C s^{-1}.[53] Therefore, our current analysis is consistent with this observation; *i.e.*, that indeed, water quenching in β titanium alloys would give rise to fully retained β grain structure. However, the cooling rates involved in FSP are around 30 °C s^{-1} to 40 °C s^{-1} and depend on the location from top to bottom of the processed zone. This implies that the current samples may not have fully retained β grain structure in Beta C and Ti-185 after FSP. The CCT diagram also shows that nose time for the start of α precipitation in Beta C is more compared to that of Ti-185. In other words, the faster kinetics of precipitation in Ti185 compared to Beta C is attributed to the presence of heavier alloying elements in Beta C, thus making the overall diffusion rate slower. This condition is further corroborated by the presence of heterogeneous nucleation in Beta C and homogenous nucleation in Ti-185 for the same aging time and temperatures. This approach can be used to develop better FSP strategy with proper selection of titanium alloys based on CCT diagram and potential of post-processing aging response.

IV. CONCLUSIONS

The wider processing window of β-titanium alloys offers potential for obtaining unique strength ductility combinations. Following conclusions can be made from the present work:

1. The tensile properties in Beta C are greater in the higher heat input condition compared to those of the lower heat input condition and were measured theoretically and experimentally. This increase in strength is attributed to the presence of a greater density of metastable phases in the higher heat input condition.
2. Two-step aging technique further improved the mechanical properties of both alloys because of significant α precipitation inside the β matrix. The higher density of α in the lower heat input condition compared to the higher heat input condition for both alloys is understood to be because of the enhanced nucleation site density created during FSP at lower heat input condition.
3. More homogenous precipitation is observed in Ti-185 compared to Beta C because of the faster diffusion kinetics in Ti-185 than Beta C. Very fine size (50 to 120 nm) alpha platelets were responsible for a very high strength in Ti-185 after aging.
4. The current results and CCT diagram-based analysis provide a road map to achieve excellent properties in β titanium alloys. The fundamental idea is to create high dislocation density *via* FSP, quench in the metastable β phase, and to age at appropriate nose temperature to tailor the strength–ductility combination.

REFERENCES

1. I. Inagaki, T. Takechi, Y. Shirai, and N. Ariyasu: *Nippon Steel & Sumitomo Metal Tech. Rep.*, 2014, vol. 106, p. 22.
2. R.R. Boyer: *JOM*, 2010, vol. 62, pp. 21–24.
3. C. Rhodes, M. Mahoney, W. Bingel, R. Spurling, and C. Bampton: *Scr. Mater.*, 1997, vol. 36, pp. 69–75.
4. G. Liu, L. Murr, C. Niou, J. McClure, and F. Vega: *Scr. Mater.*, 1997, vol. 37, pp. 355–61.
5. Y.S. Sato, H. Kokawa, M. Enomoto, and S. Jogan: *Metall. Mater. Trans. A*, 1999, vol. 30A, pp. 2429–37.
6. Y.S. Sato, H. Takauchi, S.H.C. Park, and H. Kokawa: *Mater. Sci. Eng., A*, 2005, vol. 405, pp. 333–38.
7. M.A. Sutton, B. Yang, A.P. Reynolds, and R. Taylor: *Mater. Sci. Eng., A*, 2002, vol. 323, pp. 160–66.
8. M. Peel, A. Steuwer, M. Preuss, and P. Withers: *Acta Mater.*, 2003, vol. 51, pp. 4791–801.
9. Y. Sato, S. Park, A. Matsunaga, A. Honda, and H. Kokawa: *J. Mater. Sci.*, 2005, vol. 40, pp. 637–42.
10. S.H.C. Park, Y.S. Sato, and H. Kokawa: *Scr. Mater.*, 2003, vol. 49, pp. 161–66.
11. C. Meran: *Mater Des*, 2006, vol. 27, pp. 719–26.
12. A.J. Ramirez and M.C. Juhas: *Mat. Sci. For.*, 2003, vol. 426, pp. 2999–3004.
13. T. Lienert: *Friction Stir Welding and Processing, ASM International*, 2007, pp. 123-54.
14. A.P. Reynolds, E. Hood, and W. Tang: *Scr. Mater.*, 2005, vol. 52, pp. 491–94.
15. A. Pilchak, Z. Li, J. Fisher, A. Reynolds, M. Juhas, J. Williams, K. Jata, M. Mahoney, R. Mishra, and T. Lienert: *TMS*, PA, Warrendale, 2007, pp. 419–27.
16. A. Pilchak, M. Juhas, and J. Williams: *Metall. Mater. Trans. A*, 2007, vol. 38A, pp. 435–37.
17. S. Pasta and A.P. Reynolds: *Fatigue Fract. Eng. Mater. & Struct.*, 2008, vol. 31, pp. 569–80.
18. H. Liu, L. Zhou, and Q. Liu: *Scr. Mater.*, 2009, vol. 61, pp. 1008–11.
19. L. Zhou, H. Liu, P. Liu, and Q. Liu: *Scr. Mater.*, 2009, vol. 61, pp. 596–99.
20. H.J. Liu, L. Zhou, Y.X. Huang, and Q.W. Liu: *Mat. Sci. For*, 2010, vol. 638, pp. 1185–90.
21. Y. Zhang, Y.S. Sato, H. Kokawa, S.H.C. Park, and S. Hirano: *Mater. Sci. Eng., A*, 2008, vol. 485, pp. 448–55.
22. Y. Zhang, Y.S. Sato, H. Kokawa, S.H.C. Park, and S. Hirano: *Mater. Sci. Eng., A*, 2008, vol. 488, pp. 25–30.
23. N. Kumar, J. Rodelas, and R. Mishra: *TMS Warrendale*, 2009, pp. 45–53.
24. P. Edwards and M. Ramulu: *J Eng. Mater. Technol.*, 2010, vol. 132, p. 0310061-10.
25. D. Sanders, P. Edwards, A. Cantrell, K. Gangwar, and M. Ramulu: *JOM*, 2015, vol. 67, pp. 1054–63.
26. S. Mironov, Y. Sato, and H. Kokawa: *J. Mater. Sci. Technol.*, 2018, vol. 34, pp. 58–72.
27. P. Mashinini, I. Dinaharan, J.D.R. Selvam, and D. Hattingh: *Mater. Charact.*, 2018, vol. 139, pp. 328–36.
28. K. Gangwar and M. Ramulu: *Mater Des*, 2018, vol. 141, pp. 230–55.
29. W. Brassington and P.A. Colegrove: *Sci. Technol. Weld. Join.*, 2017, vol. 22, pp. 300–18.
30. K. Jata and A.P. Reynolds: *Metallic Materials with High Structural Efficiency*, Springer, Dordrecht, 2004, pp. 391–400.
31. S. Mironov, Y. Sato, and H. Kokawa: *Mater. Sci. Eng., A*, 2010, vol. 527, pp. 7498–7504.
32. S. Nyakana, J. Fanning, and R. Boyer: *J. Mater. Eng. perform.*, 2005, vol. 14, pp. 799–811.
33. A. Devaraj, V.V. Joshi, A. Srivastava, S. Manandhar, V. Moxson, V.A. Duz, and C. Lavender: *Nat. Commun.*, 2016, vol. 7, p. 111761-10.
34. R.S. Mishra and Z.Y. Ma: *Mater. Sci. Eng., R*, 2005, vol. 50, pp. 1–78.
35. J. Su, J. Wang, R.S. Mishra, R. Xu, and J.A. Baumann: *Mater. Sci. Eng., A*, 2013, vol. 573, pp. 67–74.
36. P. Edwards and M. Ramulu: *Sci. Technol. Weld. Join.*, 2010, vol. 15, pp. 468–72.
37. A. Rollett, F. Humphreys, G. Rohrer, and M. Hatherly: *Recrystallization and Related Annealing Phenomena*, 2nd ed., Elsevier, Amsterdam, 2004.
38. I. Weiss and S. Semiatin: *Mater. Sci. Eng., A*, 1998, vol. 243, pp. 46–65.
39. W. Burgers: *Physica*, 1934, vol. 1, pp. 561–86.
40. E. Hall: *Proc. Phys. Soc B*, 1951, vol. 64, pp. 747–53.
41. N. Petch: *J. Iron Steel Inst.*, 1953, vol. 174, pp. 25–28.
42. K. Chia, K. Jung, and H. Conrad: *Mater. Sci. Eng., A*, 2005, vol. 409, pp. 32–38.
43. M. Hansen, E. Kamen, H.D. Kessler, and D. McPherson: *JOM*, 1951, vol. 3, pp. 881–88.
44. J. Yan: Dissertation. Northwestern University, 2014, pp. 117-26.
45. E. Collings: *Metals Park Ohio*, 1984, vol. 3, pp. 134–43.
46. E. Collings: *Metals Park Ohio*, 1984, vol. 3, pp. 94–111.
47. C. Hammond and J. Nutting: *Metal Sci.*, 1977, vol. 11, pp. 474–90.
48. J.D. Cotton, R.D. Briggs, R.R. Boyer, S. Tamirisakandala, P. Russo, N. Shchetnikov, and J.C. Fanning: *JOM*, 2015, vol. 67, pp. 1281–1303.
49. G. Lütjering and J.C. Williams: *Titanium*, 1st ed., Springer, Berlin, 2003.
50. F. Prima, J. Debuigne, M. Boliveau, and D. Ansel: *J. Mater. Sci. Lett.*, 2000, vol. 19, pp. 2219–21.
51. C. Yolton, F. Froes, and R. Malone: *Metall. Mater. Trans. A*, 1979, vol. 10, pp. 132–34.
52. A. Pilchak, W. Tang, H. Sahiner, A.P. Reynolds, and J. Williams: *Metall. Mater. Trans. A*, 2011, vol. 42, pp. 745–62.
53. R.S. Mishra, P. De Sarathi, and N. Kumar: *Friction Stir Welding and Processing*, Springer, Cham, 2014, pp. 189–235.